

# $4 \times 25$ Gbps Polarization Diversity Silicon Photonics Receiver With Transfer Printed III-V Photodiodes

Grigorij Muliuk<sup>ID</sup>, Student Member, IEEE, Kasper Van Gasse<sup>ID</sup>, Student Member, IEEE,  
Joris Van Kerrebrouck<sup>ID</sup>, Student Member, IEEE, Antonio José Trindade,  
Brian Corbett<sup>ID</sup>, Senior Member, IEEE, Dries Van Thourhout<sup>ID</sup>, Senior Member, IEEE,  
and Günther Roelkens<sup>ID</sup>, Senior Member, IEEE

**Abstract**—We demonstrate the transfer-printing-based integration of III-V substrate-illuminated p-i-n photodetectors onto a 4-wavelength-channel silicon photonics polarization diversity receiver circuit.  $4 \times 25$  Gbps operation is demonstrated for 2.5-nm wavelength channel spacing in the C-band. Transfer printing is an enabling technology for massively parallel heterogeneous III-V-on-Si integration.

**Index Terms**—Heterogeneous integration, transfer printing, wavelength division multiplexing receiver.

## I. INTRODUCTION

TRANSFER printing [1] is an attractive novel technology for heterogeneously integrating III-V opto-electronic devices on a silicon photonics platform. The technology combines the advantages of flip-chip integration (integration of pre-fabricated and pre-tested opto-electronic components) and die-to-wafer bonding (massively parallel integration). In comparison to flip-chipping, the simultaneous integration of arrays of devices is possible, enabling a high throughput process. In comparison to wafer bonding, the silicon photonic process flow is not disturbed by the integration of the III-V devices and the III-V processing can be done on the III-V source wafer.

Transfer printing is a versatile technology that works by releasing the III-V devices from their source substrate, picking arrays of those devices using a structured elastomeric polydimethylsiloxane (PDMS) stamp [2] and printing them on a

Manuscript received October 15, 2018; revised December 5, 2018; accepted December 22, 2018. Date of publication December 27, 2018; date of current version January 29, 2019. This work was supported by the European Union's Horizon 2020 Research and Innovation Program under Grant 645314 (TOP-HIT). (Corresponding author: Grigorij Muliuk.)

G. Muliuk, K. Van Gasse, D. Van Thourhout, and G. Roelkens are with the Center of Nano- and Biophotonics, Photonics Research Group, Department of Information Technology, Ghent University-imec, B-9052 Ghent, Belgium (e-mail: grigorij.muliuk@ugent.be; kasper.vangasse@ugent.be; dries.vanthurhout@ugent.be; gunther.roelkens@ugent.be).

J. Van Kerrebrouck is with the Center of Nano- and Biophotonics, Intec Design Group, Department of Information Technology, Ghent University-imec, B-9052 Ghent, Belgium (e-mail: joris.vankerrebrouck@ugent.be).

A. J. Trindade is with X-Celeprint Ltd., Cork T12R5CD, Ireland (e-mail: ajosetrindade@x-celeprint.com).

B. Corbett is with the Tyndall National Institute, Cork T12R5CD, Ireland (e-mail: brian.corbett@tyndall.ie).

Color versions of one or more of the figures in this letter are available online at <http://ieeexplore.ieee.org>.

Digital Object Identifier 10.1109/LPT.2018.2889901

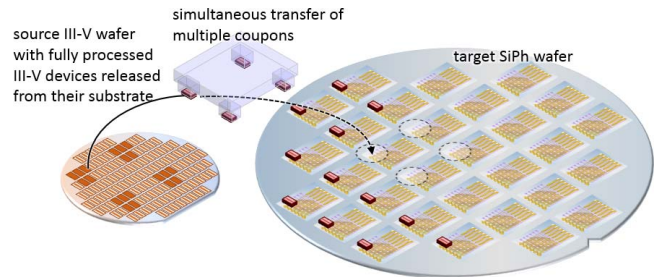


Fig. 1. Principle of transfer printing III-V opto-electronic components on a silicon photonic target wafer.

passive silicon photonics target wafer with high alignment accuracy (better than  $\pm 1.5 \mu\text{m}$ ,  $3\sigma$  [3]). This way these active devices can be integrated in a massively parallel way and potentially in a sparse manner at low cost on 200 mm or 300 mm passive silicon photonics wafers (Fig. 1).

In this letter we present an example of such an approach, namely the transfer printing of C-band substrate-illuminated III-V photodetectors on a silicon photonics 4-channel polarization diversity wavelength demultiplexer. This work is an extension of the previously demonstrated  $4 \times 25$  Gbps single polarization receiver with transfer printed photodiodes [4]. We discuss the receiver design, the transfer printing of the III-V photodiodes, the post-processing as well as the device characterization. We report  $4 \times 25$  Gbps operation below the hard-decision forward error correction (HD-FEC) threshold for both states of polarization for 4 wavelength channels in the C-band spaced by 2.5 nm.

## II. RECEIVER DESIGN

The 4-channel polarization diversity receiver design is depicted in Fig. 2 and was designed in imec's passive technology platform using a 220 nm thick silicon device layer, 70 nm, 150 nm and 220 nm etch depths and a 1.2  $\mu\text{m}$  thick top oxide cladding [5]. The light couples into the chip using a 2D grating coupler ( $-6 \text{ dB}$  coupling efficiency at 1550 nm, 40 nm 3dB bandwidth), which is etched 70 nm deep.

It splits the two polarization states at the input grating coupler and also combines both polarizations at the

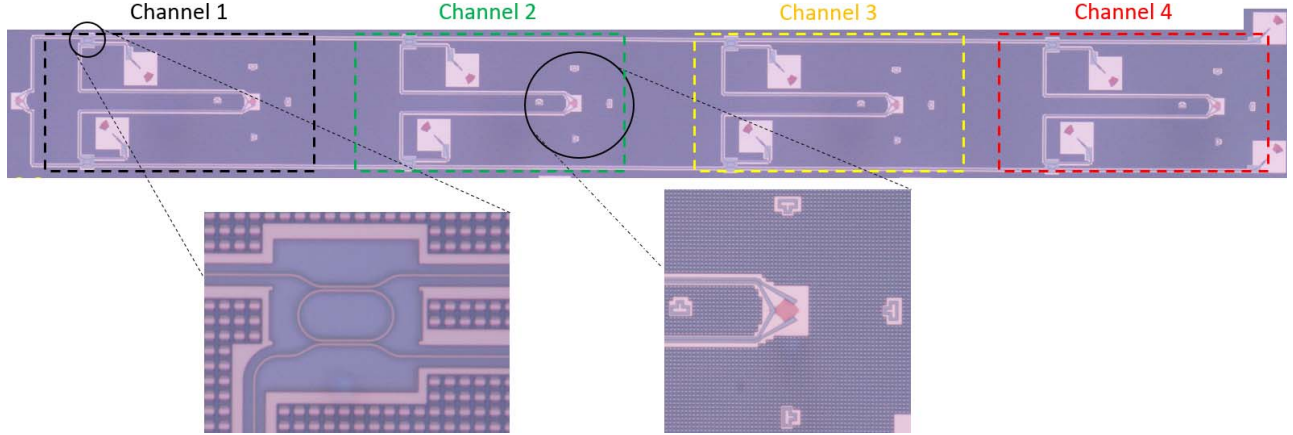


Fig. 2. Microscope image of the passive 4-channel polarization multiplexed receiver circuit with a zoom-in on a ring filter and a 2D grating coupler to interface with a transfer printed photodiode.

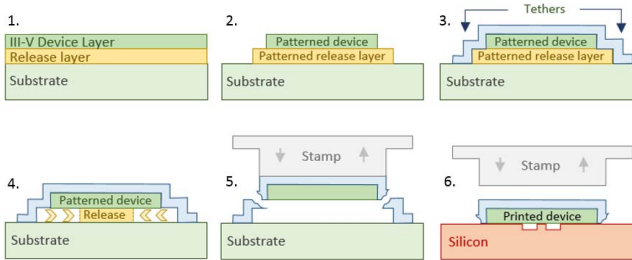


Fig. 3. Process sequence on the III-V source wafer, including the device patterning, release and transfer printing.

transfer-printed photodiode. Thermally tuned add-drop ring resonator filters (fully etched) were used for wavelength demultiplexing. The receiver makes use of 8 identical rings with  $5\ \mu\text{m}$  radius and  $9\ \mu\text{m}$  directional coupler length. The gap between the bus waveguides and the ring is chosen to be 295 nm. The Q-factor of the ring resonators is 4200 (3dB bandwidth of 370 pm) and their free-spectral range (FSR) is 10.7 nm. On-resonance the insertion loss of the ring resonators is 0.5 dB. The resonance wavelength of the rings is tuned through the integration of micro-heaters ( $200\ \mu\text{m}$  long,  $2\ \mu\text{m}$  wide and  $100\ \text{nm}$  thick spiral-shaped Ti heaters connected to  $800\ \text{nm}$  thick Au tracks).

### III. RECEIVER FABRICATION AND POST-PROCESSING

In this work we transfer printed C-band p-i-n photodiodes with an InGaAs absorption layer and with  $10\ \mu\text{m}$  diameter circular aperture. The layer stack was grown on a 500 nm thick InAlAs release layer and devices were delivered on 2 inch wafers. The specific device processing on the source wafer needed to make the devices printable is schematically illustrated in Fig. 3. The devices were made transfer-printing-compatible by defining  $75\ \mu\text{m}$  by  $75\ \mu\text{m}$  coupons by etching through the device layer stack to reach the InAlAs release layer (thereby also cutting through the device bondpads on the III-V source wafer). Secondly, the release layer is patterned using inductively coupled plasma (ICP) ( $\text{CF}_4/\text{H}_2$ , 30 min) and the devices are encapsulated with  $\sim 3\ \mu\text{m}$  thick photoresist. The photoresist is patterned in order to define tether structures that will anchor the devices to the InP substrate during the

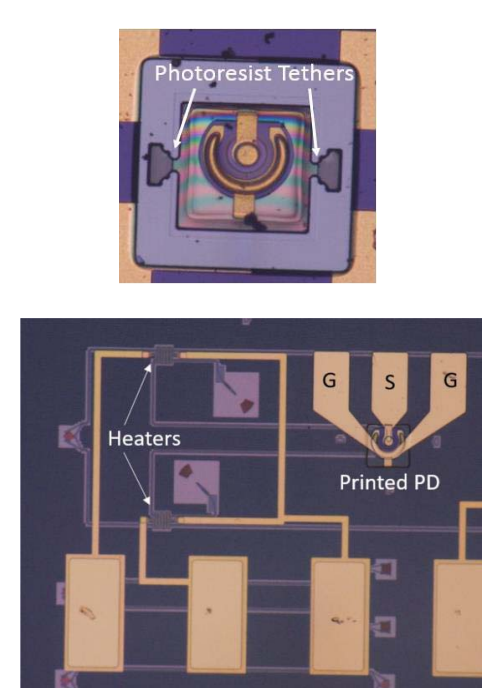


Fig. 4. (a) Microscope image of a single photodetector released from and anchored to the III-V substrate; (b) single receiver channel after transfer printing and device post-processing.

release process, while at the same time exposing the InAlAs release layer. Finally, the devices are released from the InP substrate by underetching the InAlAs release layer using  $\text{FeCl}_3:\text{H}_2\text{O}$  (1:2) at  $6\ ^\circ\text{C}$  for  $\sim 38$  minutes. More information about III-V device transfer printing development can be found in [6]–[8]. A microscope image of a single released photodiode is shown in Fig. 4 (a).

The photodiodes were printed on top of the 4 2D output grating couplers of the silicon photonics receiver, using a 50 nm thick spin-coated divinyl-siloxane-bis-benzocyclobutene (DVS-BCB) adhesive bonding agent, which was partially cured at  $180^\circ\text{C}$ . The transfer printing and post-processing was performed on  $2 \times 2\ \text{cm}$  SOI dies. The transfer printing was performed using an X-Celeprint micro-TP100 lab-scale printer. Photodiodes were sequentially printed on

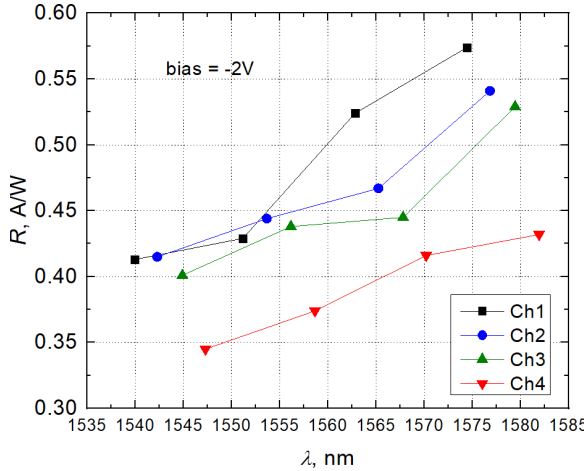


Fig. 5. Waveguide-referred responsivity measurement as a function of wavelength (-2 V bias) for all 4 channels of the receiver.

top of the 2D grating couplers. By laminating a photodetector coupon to a structured elastomeric PDMS stamp and quickly moving it in the vertical direction, one can pick up the released III-V device from the source wafer by breaking the photoresist tethers. By hovering the stamp in close proximity of the target wafer ( $\sim 100 \mu\text{m}$  separation between the coupon and the silicon photonic target wafer), the devices can be auto-aligned using COGNEX™ image recognition software [9]. To achieve high-alignment accuracy transfer printing, Tetris-brick alignment markers were incorporated in the silicon device layer (see Fig. 2), such that the geometric center coincides with the center of the circular mesa of the photodiode. The printing was performed by laminating the device against the target wafer and slowly retracting the stamp vertically, thereby leaving the coupon adhering to the target wafer. From our previous work we expect an alignment accuracy better than  $1 \mu\text{m}$  [10]. After the printing, the photoresist encapsulation of the coupons was removed using an  $\text{O}_2$  plasma.

A  $4 \mu\text{m}$  thick DVS-BCB layer was spin-coated and fully cured at  $280^\circ\text{C}$  to passivate the devices. Using an  $\text{SF}_6/\text{O}_2$  plasma the DVS-BCB layer was etched back to expose the contacts of the photodiodes as well as the heater pads after which  $1 \mu\text{m}$  thick Au ground-signal-ground contact pads were deposited for the high-speed probing of the photodiodes. Fig. 4(b) depicts the first channel of the receiver after completing the post-processing.

#### IV. MEASUREMENT RESULTS

The 4 channels of the receiver were characterized, both statically and dynamically. The dark current of the devices is about  $20 \text{ nA}$  at  $-2\text{V}$  bias, while the series resistance is  $\sim 4 \Omega$ . Using a Santec TSL-510 C-band tunable laser (TL) the waveguide-referred responsivity was measured for each channel. The result is displayed in Fig. 5. A responsivity beyond  $0.40 \text{ A/W}$  from  $1540 \text{ nm}$  to  $1585 \text{ nm}$  for channels 1, 2 and 3 and above  $0.30 \text{ A/W}$  for channel 4 is obtained, increasing with the wavelength. This increase is attributed to the increasing directionality of the output grating coupler for longer wavelengths. The slightly lower responsivity of the 4<sup>th</sup> channel is attributed to the off-resonance insertion loss

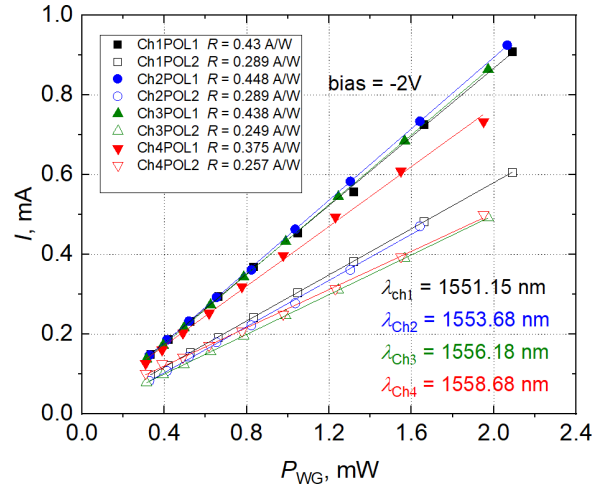


Fig. 6. Photocurrent as a function of waveguide-coupled power for the 4 channels and for the two states of polarization resulting in maximum and minimum signal (-2 V bias). The ratio of the responsivity yields the polarization dependent losses.

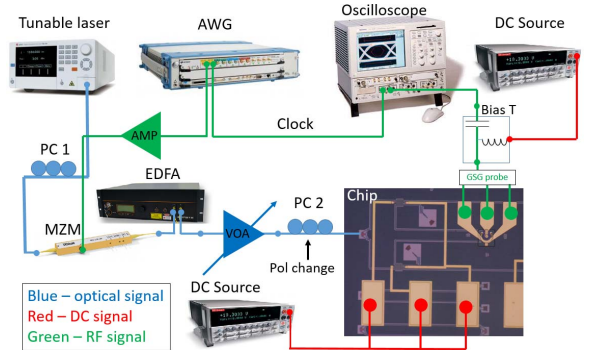


Fig. 7. Setup for large signal measurements.

of the ring resonators of channel 1-3. The resonance wavelength of the ring resonators in both arms of the polarization diversity circuit were aligned by applying a DC voltage on the integrated micro-heaters. 2.5 nm channel spacing is obtained.

Polarization dependent losses were estimated by measuring the received photocurrent versus the coupled optical power in the waveguide at the wavelengths of  $1551.18 \text{ nm}$ ,  $1553.68 \text{ nm}$ ,  $1556.18 \text{ nm}$  and  $1558.68 \text{ nm}$  for each channel respectively. After measuring the maximum photocurrent value (polarization state 1) the polarization controller position was changed to obtain the minimum photocurrent value (polarization state 2) not changing the position of the fiber. The result is displayed in Fig. 6. An average polarization dependent loss (ratio of the responsivity for the two polarization states) of 2 dB is estimated.

Small-signal measurements were carried out to assess the bandwidth of the transfer printed photodiodes, using a vector network analyzer. A 3dB bandwidth of 8 GHz is measured for the transfer printed photodiodes. The lower bandwidth can be attributed to the sub-optimal via opening and metallization on the silicon photonic target substrate.

The large signal measurement schematics are displayed in Fig. 7. The optical part consists of the TL+ Mach-Zehnder modulator (MZM), connected to an erbium-doped fiber

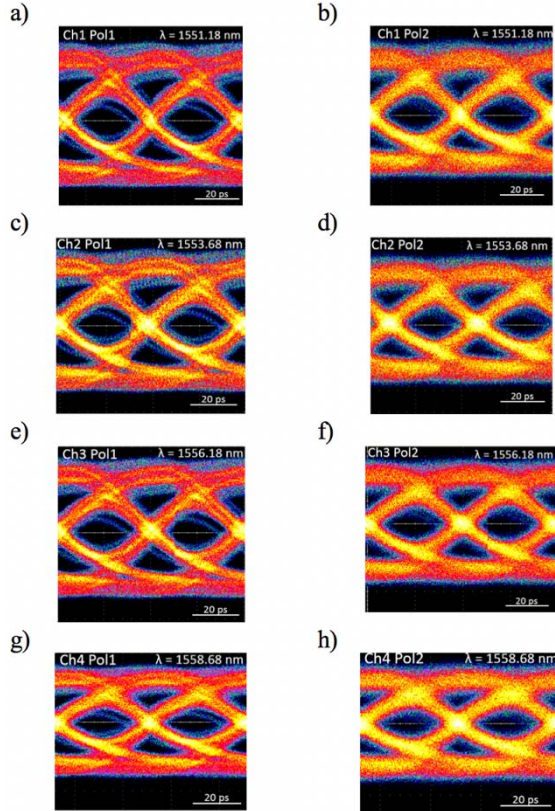


Fig. 8. 25Gbps eye diagrams for each channel for the two orthogonal polarization states. The rows indicate the different channels, the columns the two polarization states.

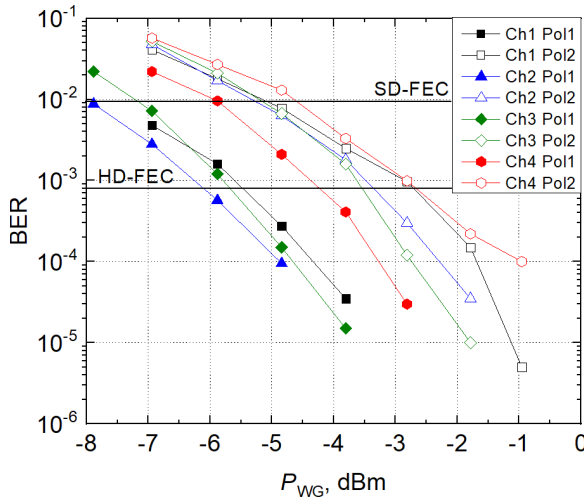


Fig. 9. BER measurements for the 4-channel receiver for both polarization states.

amplifier (EDFA) generating a fixed 15 dBm optical input power to the receiver chip (without optical attenuation). An arbitrary waveform generator (AWG) drives the MZM by

applying a pseudo-random-bit-sequence (PRBS) root-raised cosine (RRC) filtered signal with a pattern length of  $2^7\text{-}1$  at 25 Gbps. The eye-diagrams of the four channels were measured by probing the devices and using a Tektronix CSA8000 oscilloscope. Open eye diagrams were measured for all 4 channels (at wavelengths of 1551.18 nm, 1553.68 nm, 1556.18 nm and 1558.68 nm respectively) and for both polarization states as shown in Fig. 8. Using a real-time oscilloscope and a variable optical attenuator (VOA) bit-error rate curves for each channel and for both polarization states were measured. Fig. 9 shows that at 25 Gbps transmission below the hard-decision forward-error correction (HD-FEC) threshold is obtained at about  $-5.5$  dBm average waveguide-referred input power for channels 1, 2 and 3 and  $-4.25$  dBm for channel 4 for the polarization state 1.

## V. CONCLUSIONS

In this letter we demonstrate a polarization diversity 4 wavelength channel receiver (2.5 nm channel spacing) with transfer-printed III-V p-i-n detectors. This demonstration showcases the potential of transfer printing technology for the cost- and time-effective realization of active photonic integrated circuits based on silicon photonic passive waveguide circuits. The concept is not limited to the integration of photodetectors but also enables the integration of other III-V devices including lasers and even Group IV devices.

## REFERENCES

- [1] X. Feng *et al.*, "Competing fracture in kinetically controlled transfer printing," *Langmuir*, vol. 23, no. 25, pp. 12555–12560, 2007.
- [2] D. Gomez *et al.*, "Scalability and yield in elastomer stamp micro-transfer-printing," in *Proc. IEEE 67th Electron. Compon. Technol. Conf.*, Orlando, FL, USA, May/Jun. 2017, pp. 1779–1785.
- [3] D. Gomez *et al.*, "Process capability and elastomer stamp lifetime in micro transfer printing," in *Proc. IEEE 66th Electron. Compon. Technol. Conf.*, Las Vegas, NV, USA, May/Jun. 2016, pp. 681–687.
- [4] G. Muliuk *et al.*, " $4 \times 25$ Gbit/s silicon photonics tunable receiver using transfer printed III-V photodiodes," in *Proc. 31st IEEE Photon. Conf.*, Reston, VA, USA, Apr. 2018, pp. 169–170.
- [5] IMEC-EpixFAB. Accessed: Aug. 2018. [Online]. Available: [http://www.europractice-ic.com/SiPhotronics\\_technology\\_imec\\_passives.php](http://www.europractice-ic.com/SiPhotronics_technology_imec_passives.php)
- [6] A. De Groote, "Transfer-printing-based integration of single-mode waveguide-coupled III-V-on-silicon broadband light emitters," *Opt. Express*, vol. 24, no. 13, pp. 13754–13762, 2016.
- [7] J. Zhang *et al.*, "Silicon photonics fiber-to-the-home transceiver array based on transfer-printing-based integration of III-V photodetectors," *Opt. Express*, vol. 25, no. 13, pp. 14290–14299, 2017.
- [8] J. O'Callaghan *et al.*, "Comparison of InGaAs and InAlAs sacrificial layers for release of InP-based devices," *Opt. Mater. Express*, vol. 7, no. 12, pp. 4408–4414, 2017.
- [9] Cognex Vision Pro Machine Vision. Accessed: Aug. 2017. [Online]. Available: <http://www.cognex.com/products/machine-vision/visionprovision-software/>
- [10] N. Ye *et al.*, "Transfer print integration of waveguide-coupled germanium photodiodes onto passive silicon photonic ICs," *J. Lightw. Technol.*, vol. 36, no. 5, pp. 1249–1254, Mar. 1, 2018.